Available online at www.sciencedirect.com
SCIENCE DIRECT®
Journal of Catalysis 225 (2004) 337–349
JOURNAL OF CATALYSIS
www.elsevier.com/locate/jcat

Oxidation of sulfur dioxide over supported solid V_2O_5/SiO_2 and supported molten salt V_2O_5–Cs_2SO_4/SiO_2 catalysts: molecular structure and reactivity

Ioanna Giakoumelou,[a] Vasile Parvulescu,[b] and Soghomon Boghosian [a,*]

[a] *Department of Chemical Engineering, University of Patras and Institute of Chemical Engineering and High Temperature Chemical Processes (FORTH/ICE-HT), GR-26500 Patras, Greece*

[b] *University of Bucharest, Department of Chemical Technology and Catalysis, Bucharest 70346, Romania*

Received 8 April 2004; accepted 13 April 2004

Abstract

The molecular structure and reactivity of supported *solid* V_2O_5/SiO_2 catalysts with 6.5 wt% V content and surface densities in the range 0.97–2.04 V atoms/nm^2 have been studied by in situ Raman spectroscopy and activity measurements for the oxidation of SO_2. Different sol–gel routes, resulting in variations of surface area and pore volume, were used for preparing the catalysts. These catalysts were found to be practically inactive for the oxidation of SO_2 while their molecular structure evolves from isolated distorted tetrahedral O=V–(O–Si)$_3$ units exhibiting the characteristic Raman band due to V=O terminal stretch at 1032–1035 cm^{-1} to bulk V_2O_5 crystals when vanadia loading exceeds the maximum coverage of surface vanadium oxide species on silica. Promotion of the catalysts with cesium (by impregnation with Cs_2SO_4 at Cs:V = 3) results in thorough structural transformation of the studied materials which is followed by dramatic improvements in their reactivity for SO_2 oxidation. Amorphous and crystalline vanadia is extracted during calcination and dissolved in a sulfate molten salt, which remains distributed at the surface of the silica support. In situ Raman spectroscopy shows that vanadium occurs in the sulfate molten salt predominantly in the form of the mononuclear $V^VO_2(SO_4)_2^{3-}$ molten oxosulfato complex (with characteristic bands at 1034 cm^{-1} due to ν(V=O) and 942 cm^{-1} due to sulfate). A fairly good correlation between the surface areas of V_2O_5/SiO_2 precursors and TOF (turnover frequency) values was found for the V_2O_5–Cs_2SO_4/SiO_2 *molten salt* catalysts. Activation of these catalysts, following exposure to a $SO_2/O_2/N_2$ mixture, results in uptake of SO_3 and formation of a pyrosulfate molten salt, in which—as shown by the in situ Raman spectra—vanadium occurs predominantly in the form of the binuclear $(V^VO)_2O(SO_4)_4^{4-}$ molten oxosulfato complex (with characteristic bands at 1046 cm^{-1} due to ν(V=O), 830 cm^{-1} due to ν(S–O–V) and 770 cm^{-1} due to V–O–V). Exposure of the catalysts to reducing atmosphere, i.e., SO_2/N_2, results in formation of V^{IV} species, which are catalytically inactive for the oxidation of SO_2. The results should be very useful for an understanding of the structure/activity relationships in V_2O_5–Cs_2SO_4/SiO_2 molten salt catalysts.

Keywords: SO_2 oxidation; Molten salt catalysts; Vanadia catalysts; In situ Raman spectroscopy; Vanadium oxosulfato complexes; Vanadia–silica catalysts

1. Introduction

Emissions of sulfur dioxide to the atmosphere have a very significant environmental impact. The main source of such emissions is the coal-fired power generation, which is responsible for two-thirds of the 25 billion kg emitted annually in the United States. Furthermore, large amounts of SO_2 are also emitted from sulfuric acid manufacturers and smelters of nonferrous metals (245 million kg and 1.2 billion kg, respectively, according to the EPA report 454/R-00-002, March 2000) as well as from petroleum refineries and fossil fuel combustion stations. The majority of extant technologies used for SO_2 removal generate considerable amounts of waste by-products. The emerging alternative procedure for catalytic removal (oxidation to SO_3) has been applied already from the 1990s and recovers sulfur oxides in the form of concentrated sulfuric acid, as in the case of the so-called Haldor–Topsøe SNOX process, which is combined with SCR technology for NO_x removal [1]. Thus, SO_2 ox-

* Corresponding author.
E-mail address: bogosian@terpsi.iceht.forth.gr (S. Boghosian).

0021-9517/$ – see front matter
doi:10.1016/j.jcat.2004.04.012

idation catalysts are important not only for the traditional sulfuric acid manufacture but also for the catalytic removal of SO_2 from industrial gas effluents.

The catalyst used for sulfuric acid production, catalyzing the reaction $SO_2 + \frac{1}{2}O_2 \rightarrow SO_3$, contains its active vanadia phase in a molten pyrosulfate salt which is distributed in the pores of an inert silica support [2]. The literature has abundant rate equations developed for the catalytic oxidation of SO_2 [3]. Worth mentioning is the renowned Boreskov rate equation implying a first-order dependence on O_2 partial pressure [4]. The catalyst is usually made by calcination of silica (diatomaceous earth), vanadium pentoxide (or other vanadium precursors), and alkali promoters (usually in the form of sulfates) with an alkali-to-vanadium atomic ratio between 2 and 5 [2,5]. After calcination, vanadium pentoxide (vanadia) is dissolved in molten sulfate salts, which cover the catalyst surface. During use for SO_2 oxidation, the active molten sulfate phase takes up SO_3 and is best represented by the model system of vanadia dissolved in molten alkali pyrosulfates, in which the predominant species formed are vanadium oxosulfato complexes. Therefore, in order to achieve an understanding of the SO_2 oxidation catalyst operation and of the reaction mechanism, it has been considered necessary to investigate the *unsupported* molten salt/gas system V_2O_5–$M_2S_2O_7$–M_2SO_4/SO_2–SO_3–O_2–N_2 (M = Na, K, Cs, or mixtures of these) that was recognized as a realistic model of the active (molten) catalyst phase, which is distributed in the surface and the carrier pores of the catalysts.

Following a landmark article [6] initiating a systematic study of complex formation of V^V in pyrosulfate melts (without the presence of the catalyst carrier), a number of methods including potentiometry, cryoscopy, spectrophotometry, calorimetry, conductometry, cyclic voltammetry, NMR, and Raman spectroscopy have been used to study the V^V complexes in V_2O_5–$M_2S_2O_7$–M_2SO_4 melts [6–14]. Significantly, the catalytic cycle involves only V^V species (binuclear/dimeric complexes) [5,15], while side reactions leading to reduction of V^V to the catalytically inactive V^{IV} (or V^{III}) are recognized as deactivation routes. Catalytic activity studies of SO_2 oxidation in *unsupported* V_2O_5–$M_2S_2O_7$ (M = K, Na, Cs, or mixtures of these) melts allowed the isolation of precipitating V^{IV} and V^{III} crystalline compounds from deactivated catalysts [16,17]. Thus, precipitation of V^{IV} and V^{III} crystalline compounds is responsible for the catalyst deactivation, experienced typically below $\sim 440\,^\circ C$ and high catalytic activity is related to the ability of the catalyst to stabilize vanadium in the +5 oxidation state and maintain the $V^V \leftrightarrow V^{IV}$ equilibrium shifted to the left. The complex chemistry of V^{IV} and the equilibrium $V^V \leftrightarrow V^{IV}$ in the molten salt–gas system V_2O_5–$M_2S_2O_7$–M_2SO_4/SO_2–O_2–SO_3–N_2 (M = K, Cs) has been studied by high-temperature VIS/NIR, Raman and ESR spectroscopies, and potentiometry [14,18,19]. Of particular interest has been the use of high-temperature Raman spectroscopy, which enabled for the first time the establishment of the molecular structure of vanadium oxosulfato complexes present in the unsupported V_2O_5–$Cs_2S_2O_7$–Cs_2SO_4/O_2 [12], V_2O_5–M_2SO_4/O_2 (M = K or Cs) [13], and V_2O_5–$M_2S_2O_7$–M_2SO_4/SO_2–O_2 (M = K or Cs) [14] molten salt/gas systems. The resulting knowledge enables a progress in the mechanistic understanding of SO_2 oxidation [5].

In situ real-time spectroscopic characterization of catalytically active centers in vanadium oxide based SO_2 oxidation catalysts under gas and temperature conditions of practical importance has been a long-sought goal. Recently, we have been concerned with studying the molecular structure and structure/activity relationships of supported vanadia SO_2 oxidation catalysts in order to find out if the molecular structure of vanadium species present in the surface of supported molten salt SO_2 oxidation catalysts could be studied by in situ Raman spectroscopy and related to the molecular structures of the molten vanadium oxosulfato complexes studied by us previously [12–14]. Our preliminary endeavors led to the first in situ Raman study of vanadia-based SO_2 oxidation catalysts and to a comprehensive study of the molecular structure of industrial sulfuric acid catalysts [20,21]. To our knowledge, these were the first papers reporting in situ Raman study of *any* catalysts in SO_2 atmosphere.

On the other hand, the oxidation of SO_2 to SO_3 is undesirable in the conventional SCR technology in which nitrogen oxides (emitted, e.g., from coal-fired power plants) are removed catalytically over solid-state-supported vanadia catalysts [22]. If SO_2 is oxidized to SO_3, it reacts with ammonia below 250 °C to form ammonium sulfates that can block the catalyst's pores and foul downstream heat exchangers [23]. To suppress this reaction, usually the loading of vanadium is kept low and in this way the operating temperatures can be extended to lower limits (usually the flue gases are heated to 380 °C in conventional SCR). Because of the concern on reaction kinetics and on the mechanism of the catalytic oxidation of SO_2 over SCR catalysts it is desirable to design SCR catalysts able to suppress the oxidation to SO_3 and allow low SCR operating temperatures [24].

An additional problem encountered in SO_2 removal from flue gases arises from their low SO_2 content (max 3%, e.g., in the case of metallurgical plants). The amount of heat generated during the exothermic reaction in the contact process allows the reactor to operate autothermally; however, such an autothermic operation is not ensured in case of dilute gases. Means of enhancing the "low-temperature" activity of the alkali-promoted molten salt catalysts used for SO_2 oxidation included an increase of the atomic number of the alkali promoter with the use of cesium as a promoter [16,25,26]. Another possible way to enhance the efficiency of these catalysts is to use mesoporous materials as carriers, i.e., by increasing the surface area, while keeping the size of the pores in a comparable range with the traditional silica carrier of the industrial sulfuric acid catalysts.

The original interest for the present study arose from the prospect of developing high surface area V_2O_5/SiO_2 SCR catalysts with negligible activity for SO_2 oxidation and

this work is part of such a general study. The SCR reduction of NO by NH_3 has been addressed separately [27]. The present paper is concerned with the molecular structure and the catalytic properties of a series of V_2O_5/SiO_2 and V_2O_5–Cs_2SO_4/SiO_2 catalysts prepared following different sol–gel routes, for the oxidation of SO_2 contained in dilute feed gases. The catalytic activity and the structural properties were studied before and after impregnation of the vanadia/silica materials with Cs_2SO_4. Thus, in the first case the studied materials were supported solid oxide V_2O_5/SiO_2 mesoporous catalysts, and in the second case (following impregnation with Cs_2SO_4, calcination and activation) they were supported molten salt catalysts. The in situ Raman spectra obtained under oxygen, SO_2/N_2, and reaction ($SO_2/O_2/N_2$) conditions provide useful structural information and their combination with the catalytic tests contributes to an understanding of the behavior of the studied materials.

2. Experimental

2.1. Catalyst preparation and characterization

The samples studied were vanadia–silica and Cs-promoted vanadia–silica mesoporous catalysts prepared by a sol–gel process using tetraethylorthosilicate (TEOS, Aldrich > 99% pure), vanadylacetylacetonate (VAA, Aldrich, 98%) as V precursor, and Cs_2SO_4 (Merck, > 99.5%), trimethyltetradecylammonium bromide (Aldrich), HCl (Merck), ammonium hydroxide (Merck), and methanol (Merck) as reagents. Three different preparation routes were adopted.

2.1.1. Method A

VAA was dissolved in methanol with a molar ratio VAA to methanol of 0.013. TEOS was added dropwise to this solution, maintaining the system under vigorous stirring. The amount of TEOS added was calculated for molar TEOS-to-VAA ratio of 11.54 and TEOS-to-methanol ratio of 0.15. The pH of the solution was adjusted to 3 with HCl, before the addition of water (a water-to-TEOS ratio of 4) (samples A5, A8, and A9). The mixture was then refluxed at 338 K under vigorous stirring for various periods: 1 h (sample A8) or 5 h (A5, A9). Thereafter the mixture was cooled at room temperature still under vigorous stirring and refluxing. Part of these samples was mixed with a methanol solution of a quaternary salt, which was prepared by dissolution of 1 g of $(CH_3)_3C_{14}H_{29}N^+Br^-$ in 2 ml methanol. The stirring was continued for 40 min for these mixtures. The sol-polymerization and the aging of the gels were carried out either at 373 K for 5 days in a Teflon autoclave (A5) or by slow evaporation of the solvent at room temperature for 1 week (A8 and A9).

2.1.2. Method B

TEOS was dissolved in methanol with a molar ratio TEOS to methanol of 0.5 under vigorous stirring. The pH of the solution was then adjusted to 9 with a solution of NH_3(B16). The addition of water was made considering the precautions presented in method A. The system was refluxed at 353 K for 30 min under vigorous stirring. VAA was added as solution in methanol (V-to-methanol molar ratio of 0.02) after the mixture was cooled at room temperature under the same stirring conditions; 1 g $(CH_3)_3C_{14}H_{29}N^+Br^-$ in 2 ml methanol was added after 40 min vigorous stirring and the mixture was then stirred for another 40 min. The sol-polymerization and the aging of the gel were carried out at 373 K for 5 days in a Teflon autoclave.

2.1.3. Method C

TEOS was dissolved in methanol with a molar ratio TEOS to methanol of 0.5 under vigorous stirring and the pH was adjusted to 3 with HCl. Water for prehydrolysis was then added with a molar ratio water to TEOS of 2 and the mixture was refluxed at 353 K for 30 min under vigorous stirring. Separately, VAA was dissolved in methanol with a molar ratio V to methanol of 0.2 and the pH was modified with HCl to 3. Then, water for prehydrolysis was added to a molar ratio V to water of 0.043. The mixture was then refluxed for 1 h at 338 K under vigorous stirring. After cooling, the prehydrolyzed vanadium was added to prehydrolyzed TEOS and the refluxing was continued for another 2 h at 338 K, under vigorous stirring. After cooling, 1 g of $(CH_3)_3C_{14}H_{29}N^+Br^-$ in 2 ml methanol was added to the above mixture and stirred 40 min more. The sol-polymerization and the aging of the gel were carried out at 373 K for 5 days.

All samples were dried in vacuo, first at room temperature for 24 h then at 373 K for another 24 h, and finally calcined in air at 773 K using a ramp of 0.3 K min^{-1}. ICP-AES analysis indicated for all samples a vanadium content of $\sim$ 6.5 wt%.

Part of the samples (denoted as Ax, Bx, and Cx) were impregnated with cesium sulfate solution to a cesium–vanadium molar ratio of 3:1 and then dried and calcined under the same conditions used for the V_2O_5/SiO_2 catalysts. The Cs-promoted samples are denoted as AxCs, BxCs, and CxCs, respectively. The catalyst data of the samples studied in the present work are summarized in Table 1.

2.2. X-ray diffraction

The XRD patterns of the samples were recorded with a Huber Imaging Plate Guinier Camera 670, working in the highest scan resolution (0.83° min^{-1}), with the use of Cu-K_α ($\lambda = 1.5405981$ Å) radiation. The samples in powder form were finely ground and placed onto the specific diffractometer disk. The patterns were recorded at room temperature at a 2-h time scan, from 0 to 100°2θ. 20,000 data points were

Table 1
Catalyst sample data[a]

Sample	Preparation route	Gelation	Hydrogen pH	S_{BET} ($m^2\,g^{-1}$)	Average pore diameter (nm)	VO_x (nm^2)
A5	(A)	AUT	Acidic	529	3.7	1.45
A8	(A)	EVAP	Acidic	789	3.5	0.97
A9	(A)	EVAP	Acidic	777	4.5	0.99
B16	(B)	AUT	Basic	373	11.0	2.04
C21	(C)	AUT	Acidic	533	3.6	1.44

[a] BET surface area and average pore diameter data pertain to catalyst samples before impregnation with Cs_2SO_4 solution at a Cs:V = 3 ratio. Catalyst samples after Cs promotion were denoted as C21Cs, A9Cs, A5Cs, B16Cs, and A8Cs.

collected for each run, thus resulting in a 2θ step resolution of 0.005°.

2.3. Catalytic activity

Activity measurements were performed in a quartz fixed-bed microreactor operating under atmospheric pressure, which was on-line-coupled with a Fisher Rousemount spectrometer in order to analyze the outlet gas composition. The samples loaded had an approximate weight (W) of 25 mg. The standard gas feed composition was 2% SO_2 and 19% O_2 balanced in N_2. It was introduced in the microreactor with a total flow rate (F) of 100 cm^3/min STP, thus giving a W/F ratio of 0.015 $g\,s\,cm^{-3}$. The catalytic tests were conducted in the temperature range 350–550 °C.

2.4. In situ Raman spectroscopy

Approximately 150 mg of each catalyst was pressed into a self-supporting wafer, which was mounted on a stainless-steel adjustable holder in the center of the in situ cell used for recording of the Raman spectra. The in situ cell is a kanthal-wound double-wall quartz glass tube furnace mounted on a xyz plate and possesses gas inlets and outlets as well as a thermocouple sheath in contact with the catalyst sample holder. The gases used were SO_2 (Matheson, Union Carbide 99.98% anhydrous), N_2, and O_2(both L'Air Liquide, 99.999%) mixed by using thermal mass flowmeters (Brooks Instr. Model 5850E). The gas feed consisted of 0.4% SO_2 and 4% O_2 in a balance of N_2 (percentages being molar) at a total feed flow rate of 30 cm^3/min.

Raman spectra were recorded by using the 488.0 nm line of a Spectra Physics 164 argon ion laser at a power level of 30 mW (best compromise between Raman signal, laser reflections and possible laser-induced heating), measured before its entrance in the Raman furnace. In order to reduce irradiance on samples, the laser line was focused on the sample by a cylindrical lens (slightly defocused, resulting in a ~ 2 mm^2 illuminated spot). Thus, the analyzed area was representative of the sample and this was cross-checked by analyzing also different spots on each sample, in this way confirming its homogeneity. The scattered light was collected at 90° (horizontal scattering plane), analyzed with a 0.85 m Spex 1403 double monochromator, and detected by a −20 °C cooled RCA photomultiplier equipped with EG&G photon counting electronics.

The same experimental procedure was followed in both the nonpromoted and the Cs-promoted samples. In this way, the in situ Raman spectra gave comparative views of the molecular structure of the catalysts, before and after deposition of Cs_2SO_4. Each sample was oxidized under O_2 flow for more than 2 h (the oxidation was performed at 400 °C for V_2O_5/SiO_2 catalysts and at 500 °C for V_2O_5–Cs_2SO_4/SiO_2 catalysts), and the in situ spectrum of the oxidized catalyst was recorded under flowing oxygen. The Cs-promoted catalysts were oxidized at 500 °C in order to enable vanadium oxides to react with cesium sulfate and dissolve in the molten salts, a procedure which is known to occur at 500 °C in the presence of O_2 [13]. The catalyst was then exposed to the reaction mixture ($SO_2/O_2/N_2$) overnight at 480 °C and spectra were recorded in situ at different temperatures, following 1 h of exposure to the feed gas. Finally the samples were exposed overnight to reducing atmosphere, SO_2/N_2, and in situ spectra were recorded at regular temperature intervals in order to explore the expected catalyst deactivation [5,16,17], of the Cs-containing samples. Before a change of the gas atmosphere in the above sequence, the catalyst was cycled by being subjected to oxidation in O_2 at 400 °C (V_2O_5/SiO_2 catalysts) or activation in $SO_2/O_2/N_2$ at 480 °C (V_2O_5–Cs_2SO_4/SiO_2 catalysts) and the Raman spectra corresponding to these conditions were reproduced.

3. Results and discussion

3.1. X-ray diffraction

Fig. 1 shows representative X-ray diffraction patterns of catalyst samples after calcination. Pattern a is obtained for sample B16 (V_2O_5/SiO_2) and pattern b is obtained for the Cs-promoted A5Cs (V_2O_5–Cs_2SO_4/SiO_2) sample. Pattern c obtained for pure crystalline Cs_2SO_4 is included for comparison (reproduced from Ref. [13]). The broad feature centered at $\sim$ 20–25°2θ appearing in both catalyst samples is due to the amorphous silica carrier [28]. Presence of crystalline V_2O_5 is evidenced in the nonpromoted B16 catalyst

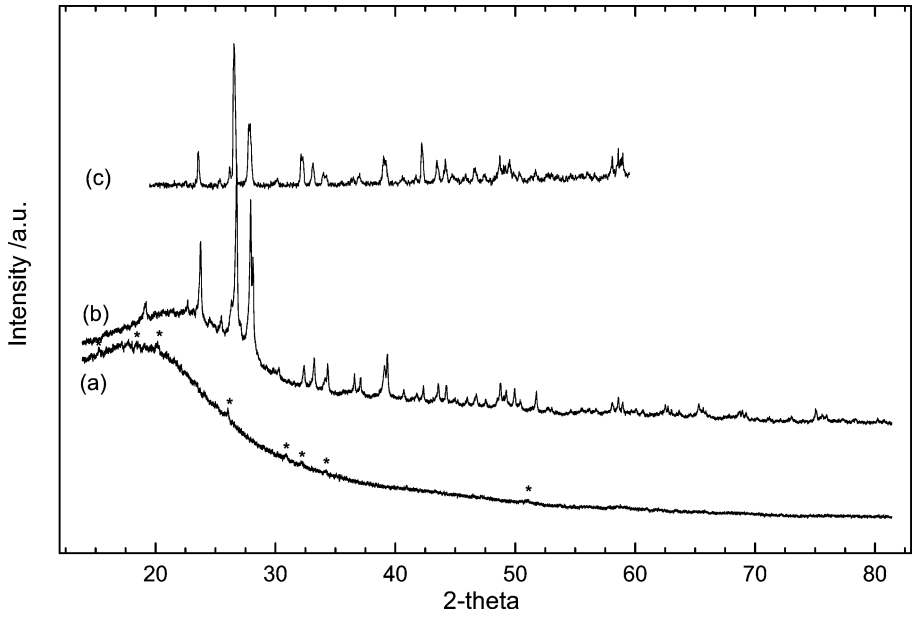

Fig. 1. X-ray diffractograms of (a) calcined V_2O_5/SiO_2 catalyst (sample B16); (b) calcined V_2O_5–Cs_2SO_4/SiO_2 catalyst (A5Cs); and (c) crystalline Cs_2SO_4. (* V_2O_5 peaks.)

by the appearance of the 15.04, 21.31, 25.83, 31.99, and 33.99° peaks. The existence of crystalline V_2O_5 in sample B16 (V_2O_5/SiO_2) is further confirmed by in situ Raman spectroscopy, as discussed below.

A comparison of patterns b and c shows that crystalline Cs_2SO_4 is present either on the surface of the Cs-promoted A5Cs catalyst or as a separated phase. The broadness of the band in pattern c is justified by the fact that this pattern is obtained earlier [13] with lower resolution. Furthermore, the pattern of A5Cs catalyst shows no evidence for presence of crystalline V_2O_5. The exploitation of the in situ Raman spectra obtained for V_2O_5/SiO_2 and V_2O_5–Cs_2SO_4/SiO_2 catalysts will shed more light in the differences observed between their molecular structures, beyond the identification of the crystalline species present.

3.2. Catalytic activity

Fig. 2 shows the TOF values measured at 475 °C for the catalyst samples studied, after impregnation with Cs_2SO_4. Nonpromoted V_2O_5/SiO_2 catalysts exhibit very low activities for the reaction of SO_2 oxidation, in agreement with Dunn et al. [24], who reported TOF values for such catalysts in the order of 10^{-6} s^{-1}. Promoting the above catalysts with Cs_2SO_4 at a Cs/V ratio of 3 led to significantly higher TOF values, as seen in Fig. 2. The positive effect of alkali metal sulfates as promoters of the vanadia catalysts for SO_2 oxidation has been demonstrated a long time ago [25]. Furthermore, increasing the atomic number of the alkali metal has a beneficial effect in the promotion of the catalyst [16,17,25]. In particular, when using Cs as a promoter, it has been shown based on kinetic data that a Cs/V ratio of 3–3.5 is optimal [26,29]. The present work will demonstrate, based on

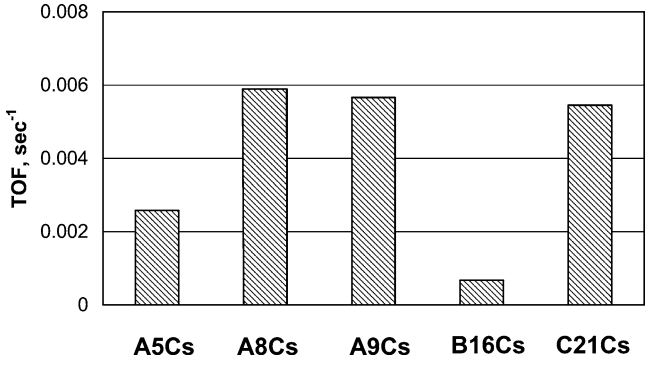

Fig. 2. Turnover frequencies (TOF) for the various V_2O_5–Cs_2SO_4/SiO_2 catalysts measured at 475 °C. Gas feed: 2% SO_2, 19% O_2, 79% N_2. $W/F = 0.015$ g s cm^{-3}.

the results obtained by in situ Raman spectroscopy, that after promotion with Cs_2SO_4 the samples behave as *supported molten salt* catalysts. The catalytic performance depends on the procedures by which the vanadia–silica support was prepared. Actually, a rather good correlation between the measured surface area of vanadia–silica precursors and the TOF was determined (see Table 1, and Fig. 2). This is not surprising, in view of the fact that the activity of supported molten salt catalysts is largely determined by the availability of active vanadium components. It should be pointed out that following promotion of the catalysts with Cs_2SO_4 and calcination, the surface area (S_{BET}) drops markedly due to filling of the carrier pores with molten salts.

The relation between the surface area of the support and the vanadia loading is well known [2,30]. An increase in the concentration of vanadia–alkali sulfate active components causes thickening of the liquid layer containing the active vanadium oxosulfato complexes, filling of wider pores,

and additional reduction in the effective surface, thus contributing to a decrease in the reaction rate. The maximum thickness of the active component film at which diffusion retardation does not occur is about 600 Å [31,32]. Such a value is suggestive of a nonuniform distribution of the active liquid phase on the carrier. The effective film thickness of the molten salt decreases with decreasing temperature and increases with increasing conversion [33]. The TOF values measured in this study confirm the importance of the surface area, since mostly a direct correlation between catalytic activity and surface area is observed. Finally, it should be pointed out that the TOF values reported in this work are obviously the *apparent* TOF values, since in both cases of supported vanadia catalysts (supported solid oxide or supported molten salt) vanadia is not 100% dispersed.

3.3. In situ Raman spectroscopy

Differences in the molecular structures of V_2O_5/SiO_2 and V_2O_5–Cs_2SO_4/SiO_2 catalysts are not restricted only to the identity of the crystalline species present, addressed in the discussion of the X-ray diffraction patterns, but also to the structure of the various surface solid oxides and molten salts occurring in the two sets of catalysts, respectively. In situ Raman spectroscopy of the catalysts under oxidation, reduction, and steady-state reaction conditions (namely O_2, SO_2/N_2, and $SO_2/O_2/N_2$, respectively) is a sensitive experimental technique for probing their molecular structures.

3.3.1. In situ Raman spectra of catalysts under oxidation conditions

3.3.1.1. V_2O_5/SiO_2 catalysts. Fig. 3 shows representative in situ Raman spectra of nonpromoted (i.e., V_2O_5/SiO_2) catalysts, namely of samples A8 and B16, of which the surface densities are 0.97 and 2.04 V atoms/nm^2, respectively. The spectra have been recorded following exposure of the catalysts in flowing oxygen for 2 h at 400 °C and represent the fully oxidized state of the catalysts under dehydrated conditions. The vanadium surface density for both samples is higher when compared to the most commonly reported maximum coverage capacity of the silica carrier (0.7 V atoms/nm^2) [34]. However, the spectrum of the A8 catalyst shows no evidence of crystalline V_2O_5 formation, even though it has a surface density of 0.97 V atoms/nm^2. This is not very surprising in view of literature reports noting that certain catalyst preparation methods can enhance the surface coverage of the vanadia species on silica to approximately up to 2–3 V atoms/nm^2 [34]. Therefore, a relatively good dispersion of vanadium must prevail as a result of the sol–gel preparation procedure used in the present study. The in situ Raman spectrum of sample B16, which has a surface density of 2.04 V atoms/nm^2 exhibits the characteristic 994 cm^{-1} band due to crystalline V_2O_5 in agreement with the XRD results (Fig. 1). The remaining features of the spectra obtained for both catalysts (shown in Fig. 3) are typical for solid-state V_2O_5/SiO_2 catalysts [35,36] exhibiting an

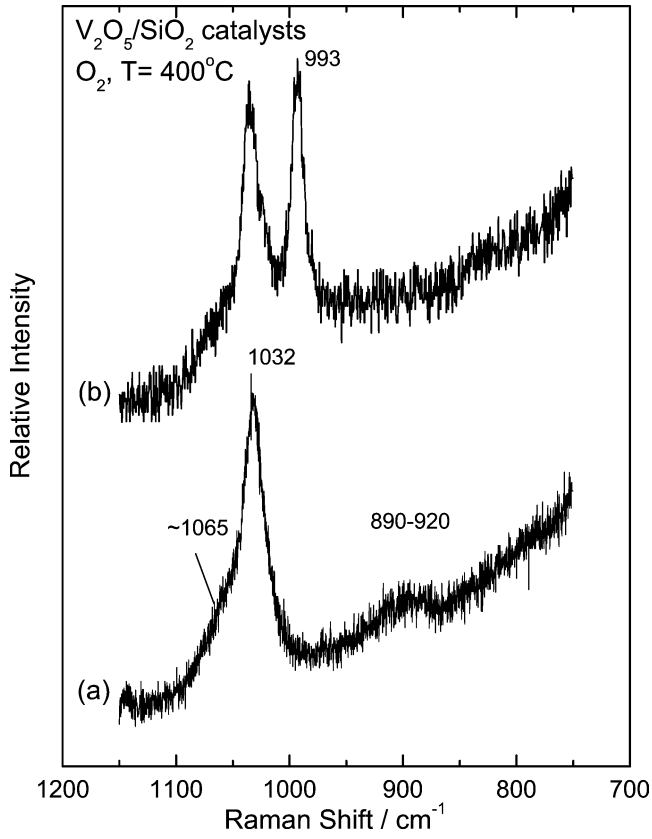

Fig. 3. In situ Raman spectra of V_2O_5/SiO_2 nonpromoted catalysts obtained under O_2 at 400 °C for (a) A8 sample; (b) B16 sample. Spectral slit width, sww = 8 cm^{-1}; scan speed, ss = 0.2 cm^{-1} s^{-1}; time constant, $\tau = 1$s.

intense peak at ∼ 1035 cm^{-1} due to V=O terminal bond vibration of isolated, distorted tetrahedral vanadyl species, possessing one V=O bond and three bridging V–O–Si bonds in a O=V–(O–Si)$_3$ configuration, as anticipated [34]. Two weaker bands can also be seen in Figs. 3a and b, namely a shoulder at ∼ 1065 and a broad band at 880–920 cm^{-1}, the latter band being smeared out in spectrum b due to lower signal-to-noise ratio. These bands are reported as characteristic of Si–O functionalities attributed to perturbed silica vibrations, which are indicative of V–O–Si bond formation [35–37]. Formation of polymeric vanadates on silica substrates is not commonly encountered in the literature. Thus, due to lower interaction of silica with vanadia, increasing loading results in the formation of crystalline V_2O_5 [36,38]. Table 2 lists the observed Raman band wavenumbers and their assignments.

3.3.1.2. V_2O_5–Cs_2SO_4/SiO_2 catalysts. The Cs-promoted catalysts were dried following the same conditions used for the nonpromoted vanadia–silica catalysts and were finally calcined at 500 °C.

Recently we have been concerned with the structural and vibrational properties of V_2O_5–M_2SO_4 (M = K, Cs) unsupported molten salts at temperatures up to 570 °C and based on the high-temperature Raman spectra obtained we have

Table 2
Observed vibrational Raman wavenumbers (cm^{-1}) in in situ Raman spectra of V_2O_5/SiO_2 solid state catalysts[a]

V_2O_5/SiO_2 400 °C, O_2 (Fig. 3)	V_2O_5/SiO_2 400 °C, $SO_2 + O_2$ (Fig. 5)	Assignment
	~ 1140 w	
~ 1065 sh	~ 1065 sh	Si–O⁻, Si(–O⁻)$_2$[b]
1032–1035 s	1032–1035 s	ν(V=O), O=V–(O–Si)$_3$
994 s	994 s	V_2O_5 (cr)[c]
880–920 br	880–920 br	Si–O⁻, Si(–O⁻)$_2$

[a] Abbreviations: s, strong; m, medium; w, weak; v, very; sh, shoulder; br, broad.
[b] Refs. [36,37].
[c] Observed for vanadium surface densities exceeding the maximum surface coverage of vanadia on silica.

achieved a thorough understanding of the molecular structure of the vanadium(V) complexes formed in these binary molten systems [13]. It thus remained to be realized if the molecular structure of the vanadium species present in the surface of supported V_2O_5–Cs_2SO_4/SiO_2 catalysts could be studied by in situ Raman spectroscopy and if their structure could be linked with that of unsupported molten salts studied by us previously [13].

Vanadium pentoxide reacts with cesium sulfate in the presence of oxygen and at 500 °C the reaction leads to a molten salt [13], which in the present case is expected to be dispersed and distributed at the surface of the silica support. It has been shown that a 2:1 Cs_2SO_4:V_2O_5 mixture ($X^0_{V_2O_5} = 0.33$) melts below 450 °C and contains $VO_2(SO_4)_2^{3-}$ and VO_3^- units in chain-like and network-like configurations, whereas further addition of sulfate results in precipitation of crystalline Cs_2SO_4 [13]. The presence of oxygen is extremely crucial, bearing in mind that on heating alkali sulfates with vanadium pentoxide in the absence of oxygen a solid state reaction occurs [39] thereby, oxygen is released and vanadium is partially reduced according to, e.g.,

$$K_2SO_4 + 6V_2O_5 \rightarrow 2KV_6O_{15} + \tfrac{1}{2}O_2 + SO_3. \quad (1)$$

Fig. 4 shows representative in situ Raman spectra obtained for catalysts samples A9Cs, A5Cs, and C21Cs at 500 °C under flowing O_2 (spectra a, b, and c). One can observe that the spectra of all catalysts possess bands at 1068, 960, and 611 cm^{-1}, which are due to the well-known $\nu_3(SO_4^{2-})$, $\nu_1(SO_4^{2-})$, and $\nu_4(SO_4^{2-})$ modes of crystalline Cs_2SO_4, respectively [13]. These bands dominate the spectra of sample A9Cs (Fig. 4a), whereas they appear weaker in the spectra of A5Cs and C21Cs. Thus, the three catalysts studied, although of similar vanadia loading and same Cs:V = 3 ratio, appear to contain different amounts of crystalline Cs_2SO_4. It is known that for $X^0_{V_2O_5} < 0.33$ crystalline Cs_2SO_4 precipitates from V_2O_5–Cs_2SO_4 molten mixtures [13] and therefore precipitation of Cs_2SO_4 is indeed expected to occur in the liquid phase of the studied catalysts, since the Cs:V = 3 ratio corresponds to $X^0_{V_2O_5} = 0.25$. On

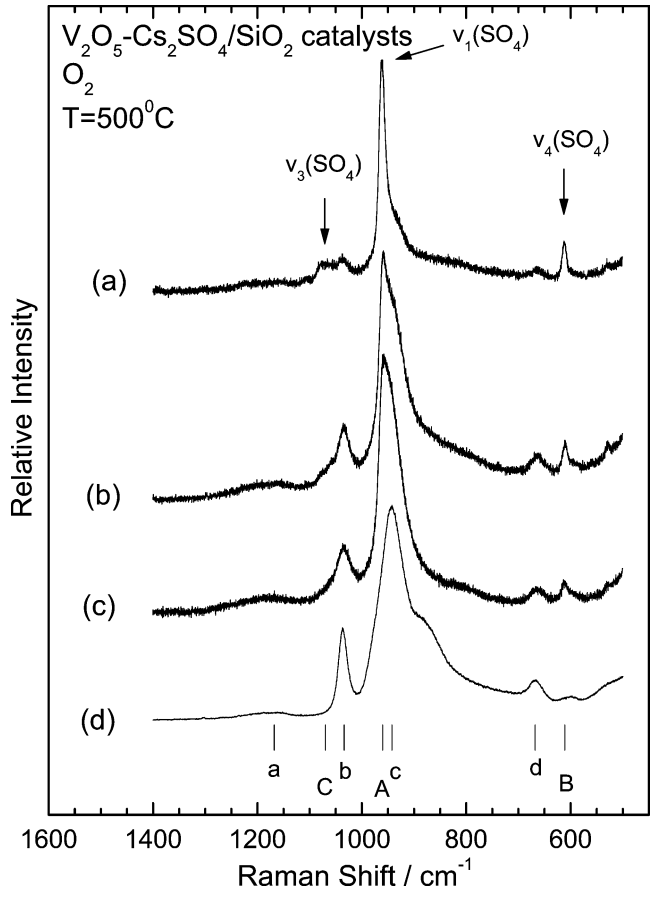

Fig. 4. In situ Raman spectra of V_2O_5–Cs_2SO_4/SiO_2 catalysts obtained under O_2 at 500 °C for (a) A9Cs; (b) A5Cs; (c) C21Cs. (d) Raman spectrum of V_2O_5–Cs_2SO_4 molten mixture (under O_2) with $X^0_{V_2O_5} = 0.33$ at 490 °C (reproduced from Ref. [13]). Recording parameters: see Fig. 3. Band notation: see Table 3.

the other hand, the variations in the relative amounts of crystalline Cs_2SO_4 are in accordance with the morphological characteristics of the catalysts (Table 1). According to these characteristics more vanadia might be available for reaction with Cs_2SO_4 at the outer catalyst surface in the case of C21Cs and A5Cs, which have smaller pores. In contrary, vanadia remains "trapped" in the larger pores of A9Cs, where Cs_2SO_4 cannot access it due to lack of mixing of the viscous molten mixtures which are distributed on the support material.

The remaining features of spectra a, b, and c (Fig. 4) are identical to the spectrum of the V_2O_5–Cs_2SO_4 molten mixture with $X^0_{V_2O_5} = 0.33$ (i.e., Cs:V = 2:1) at 490 °C, which is included in Fig. 4 (spectrum d, reproduced from Ref. [13]) to facilitate the comparison and the discussion. Thus, the spectra of the three catalysts (Figs. 4a–c) exhibit bands at ~ 1165 (weak, broad), 1036 (strong), ~ 942 cm^{-1} (obscured partly to different extents for the three catalysts from the 960 cm^{-1} band), and 668 (medium) cm^{-1}, which are known to originate from the molten V(V) complex $VO_2(SO_4)_2^{3-}$, which is the product of the reaction of vanadium oxide and cesium

Table 3
Observed vibrational Raman wavenumbers (cm^{-1}) in in situ Raman spectra of V_2O_5–Cs_2SO_4/SiO_2 molten salt catalysts[a]

Band notation (Figs. 4 and 6)	V_2O_5–Cs_2SO_4/SiO_2 500 °C, O_2	V_2O_5–Cs_2SO_4/SiO_2 480 °C, $SO_2 + O_2$	Assignment
α		1172 m	$(V^VO)_2O(SO_4)_4^{4-}$ [b]
a	1168 w		$V^VO_2(SO_4)_2^{3-}$ [c]
A′		1078 m	$\nu_1(S_2O_7^{2-})$
C	1068 w[d]		$\nu_3(SO_4^{2-})$, Cs_2SO_4 (cr)
β		1046 m	ν(V=O), $(V^VO)_2O(SO_4)_4^{4-}$ [b]
b	1034 s		ν(V=O), $V^VO_2(SO_4)_2^{3-}$ [c]
γ		994 w	ν(S–O_t), $(V^VO)_2O(SO_4)_4^{4-}$ [b]
A	961 vs sharp[d]		$\nu_1(SO_4^{2-})$, Cs_2SO_4 (cr)
c	942 s, sh		$\nu(SO_4^{2-})$, $V^VO_2(SO_4)_2^{3-}$ [c]
δ		830 s, br	ν(S–O–V), $(V^VO)_2O(SO_4)_4^{4-}$ [b]
ε		770 m, br	ν(V–O–V), $(V^VO)_2O(SO_4)_4^{4-}$ [b]
ζ		690 m	$(V^VO)_2O(SO_4)_4^{4-}$ [b]
d	668 m		$V^VO_2(SO_4)_2^{3-}$ [c]
η		666 m	$(V^VO)_2O(SO_4)_4^{4-}$ [b]
B	611 m, sharp[d]		$\nu_2(SO_4^{2-})$, Cs_2SO_4 (cr)
θ		593 w	$(V^VO)_2O(SO_4)_4^{4-}$ [b]

[a] Abbreviations: see Table 2.
[b] See Ref. [14].
[c] See Ref. [13].

sulfate [13], written as

$$V_2O_5 + 2SO_4^{2-} \rightarrow 2VO_2(SO_4)_2^{3-} + VO_3^{-}. \quad (2)$$

This reaction must be considered only as a scheme accounting for the formation of molten $VO_2(SO_4)_2^{3-}$ at the catalyst surface, since the state of vanadia present cannot be described accurately as V_2O_5. For the same reason it might be more appropriate to symbolize the second product of reaction (2) as VO_x. The structural model for this mononuclear V species is deduced based on high temperature Raman studies of the V_2O_5–M_2SO_4–$M_2S_2O_7/O_2$–SO_2 molten salt/gas systems [12–14]. Table 3 (column 2) lists the band wavenumbers observed in the in situ Raman spectra of V_2O_5–Cs_2SO_4/SiO_2 catalysts under O_2 at 500 °C.

One should expect to observe the group vibrations of VO^{3+} and SO_4^{2-} units of the $VO_2(SO_4)_2^{3-}$ V^V complex. The four sulfate fundamentals (ν_1–ν_4) for a tetrahedral T_d configuration span the representation

$$\Gamma_{vib} = A_1(\nu_1) + E(\nu_2) + 2F_2(\nu_3 + \nu_4)$$

and are well known from Raman work on aqueous solutions: $\nu_1(A_1) \approx 980\ cm^{-1}$, $\nu_2(E) \approx 450\ cm^{-1}$, $\nu_3(F_2) \approx 1100\ cm^{-1}$, and $\nu_4(F_2) \approx 615\ cm^{-1}$ [40]. However, coordination of the sulfate ion and interactions with other ions are expected to shift the bands moderately, reduce the symmetry, and lift the degeneracies of the ν_2, ν_3, and ν_4 modes. This behavior has already been observed in the Raman spectra of molten M_2SO_4–V_2O_5, $M_2S_2O_7$–V_2O_5, and $M_2S_2O_7$–M_2SO_4–V_2O_5 (M = K or Cs) mixtures [12–14]. Vertical lines in Fig. 4 mark the most prominent bands due to the various species present as follows: uppercase A–C denote bands due to crystalline Cs_2SO_4; lowercase a–d denote bands due to $VO_2(SO_4)_2^{3-}$ and the same notation is used in Table 3. The band at 1036 cm^{-1} is due to the V^V=O terminal stretch of six-coordinated vanadium of $VO_2(SO_4)_2^{3-}$ and the shoulder band at 940 cm^{-1} is due to S–O terminal stretches of sulfate in $VO_2(SO_4)_2^{3-}$ [13]. The strong shoulder band at 880 cm^{-1} observed in spectrum 4d of the molten salt mixture—and not in spectra 4a–c of the catalysts has previously been assigned to S–O–V modes along S–O–V chains of three-dimensional network-like $[VO_2(SO_4)_2]_n^{3n-}$ polymeric configurations formed in the unsupported molten salts [13]. Such extensive networking is not expected at the surface of the catalyst where the liquid/molten phase is distributed in the form of thin (100–1000 Å) films [2,31–33]. The band assignments discussed above are summarized in the last column of Table 3.

3.3.2. *In situ Raman spectra of catalysts under SO_2 oxidation reaction conditions*

3.3.2.1. V_2O_5/SiO_2 catalysts. Fig. 5 shows representative in situ Raman spectra obtained at 400 °C for the A8 sample, which has a surface density of 0.97 VO_x/nm^2, in SO_2/N_2 atmosphere (spectrum b) and in steady-state SO_2 oxidation conditions, i.e., in $SO_2/O_2/N_2$ atmosphere (spectrum c). The spectrum of the oxidized sample is also included for comparison (spectrum a). It is evident that, as seen in Fig. 5b, after overnight exposure to reducing atmosphere the 1032-cm^{-1} band due to the V=O terminal stretch of the surface monovanadate units does not undergo any shift but undergoes a slight decrease in its intensity, which is indicative of a partial reduction of V(V) to V(IV) or/and V(III). By exploiting the intensities of the 1032-cm^{-1} band due to V=O in spectra 5a and b it turns out that a ~ 20% reduction in the peak area due to surface monovanadates can be estimated in a SO_2/N_2 atmosphere.

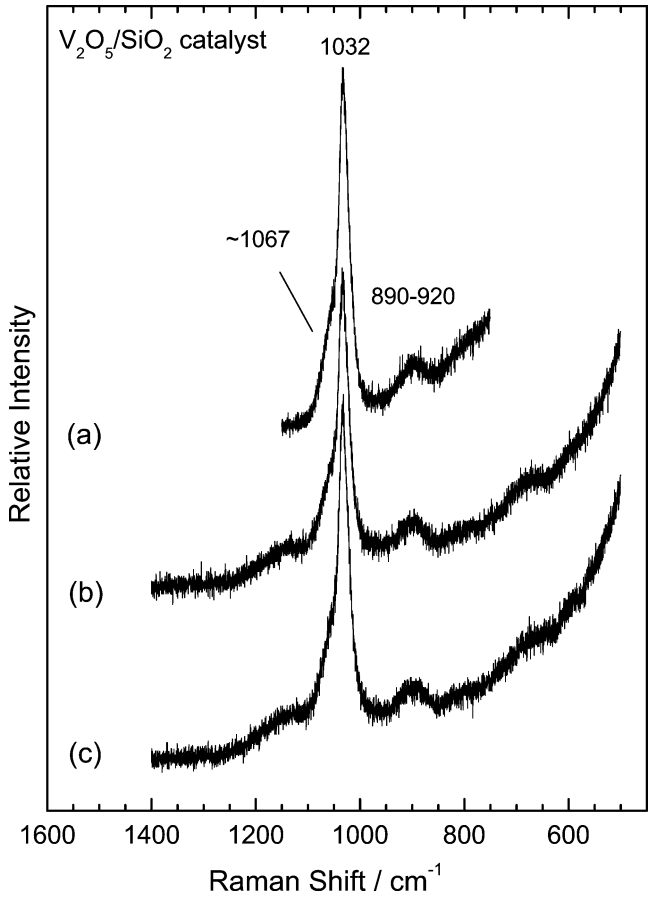

Fig. 5. In situ Raman spectra of V_2O_5/SiO_2 A8 catalyst taken at 400 °C (a) under pure O_2; (b) under SO_2/N_2 atmosphere; and (c) under $SO_2/O_2/N_2$. Recording parameters: see Fig. 3.

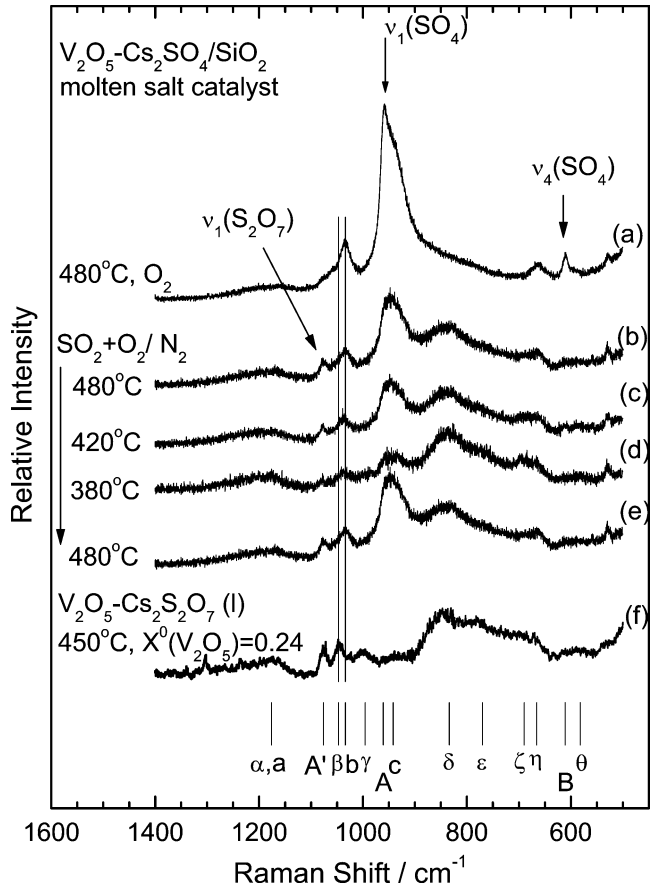

Fig. 6. (a–e) In situ Raman spectra of V_2O_5–Cs_2SO_4/SiO_2 A5Cs catalyst recorded at temperatures and atmospheres listed by each spectrum; recording parameters: see Fig. 3. (f) Raman spectrum of V_2O_5–$Cs_2S_2O_7$ molten mixture with $X^0_{V_2O_5} = 0.24$ at 450 °C. Vertical lines mark the positions of the most prominent bands due to $VO_2(SO_4)_2^{3-}$ and $(VO)_2O(SO_4)_4^{4-}$ [13,14]. Band notation: see Table 3.

During reaction conditions ($SO_2/O_2/N_2$), the in situ Raman spectrum of sample A8 exhibits the 1032 cm^{-1} with intermediate intensity when compared to the intensities of the same band in spectra 5a and b, obtained under oxidation (O_2) and reduction (SO_2/N_2) conditions, respectively. In particular a ∼ 10% reduction in the pertinent peak area can be estimated. Thus the extent of reduction of the monovanadate species, based on the intensity loss of the V=O band on going from spectra 5a to c is lower when compared to the extent of reduction evidenced on going from spectra 5a to b.

Previously, comprehensive studies of SO_2 oxidation over supported vanadia catalysts (V_2O_5/M_xO_y, M = Ce, Zr, Ti, Al, or Si), have raised the significance of the bridging V–O–M bond for the catalyst reactivity [24]. Thus, it had turned out that the more basic the bridging V–O–M bond the higher the activity toward oxidation of the acidic sulfur dioxide. This behavior correlated very well with the Sanderson electronegativities of the oxide support cations [24], in agreement to which the V_2O_5/SiO_2 catalysts exhibited the lowest reactivity. Likewise, very low TOF values (of the order of 10^{-6} s^{-1} at 400 °C) were measured in the present study.

3.3.2.2. V_2O_5–Cs_2SO_4/SiO_2 catalysts. Fig. 6 shows sequential in situ Raman spectra of the A5Cs catalyst at SO_2/O_2 atmosphere (spectra b–e) obtained at different temperatures. The in situ spectrum of the calcined catalyst under O_2 at 480 °C is included for comparison (Fig. 6a). As seen in spectrum 6b, after exposure of the sample to SO_2 and O_2 at 480 °C for 1 h, the $\nu_1$and ν_3 sulfate bands disappear and a band at 1078 cm^{-1} emerges in the spectrum. The 10-fold excess of O_2 and the low retention time are sufficient to secure that SO_2 is converted to SO_3. The observed spectral changes are then interpreted to indicate that crystalline sulfate reacts with SO_3 forming molten pyrosulfate according to

$$SO_4^{2-} + SO_3 \rightarrow S_2O_7^{2-}. \quad (3)$$

The band observed at 1078 cm^{-1} is the strongest and most characteristic band of the pyrosulfate group, $\nu_1(S_2O_7^{2-})$ [14]. Furthermore, the 770/830 cm^{-1} strong and broad feature, which is very characteristic of the molten dimeric $(VO)_2O(SO_4)_4^{4-}$ [12,14], appears in spectrum (Fig. 6b). Thus, the molten pyrosulfate formed dissolves some of the residual vanadium(V) oxides present and more-

over reacts with $VO_2(SO_4)_2^{3-}$ according to [12,14]

$$V_2O_5 + 2S_2O_7^{2-} \rightarrow (VO)_2O(SO_4)_4^{4-}, \quad (4)$$

$$VO_2(SO_4)_2^{3-} + S_2O_7^{2-} \leftrightarrow (VO)_2O(SO_4)_4^{4-} + 2SO_4^{2-}. \quad (5)$$

The 830 cm^{-1} band is due to S–O–V and the 770 cm^{-1} band is due to V–O–V of the $(VO)_2O(SO_4)_4^{4-}$ molten complex [12,14], which is considered the active species in the catalytic cycle of SO_2 oxidation [5]. In order to facilitate the discussion, the spectrum of the V_2O_5–$Cs_2S_2O_7$ molten mixture with $X^0_{V_2O_5} = 0.24$ (i.e., merely a mixture of the $(VO)_2O(SO_4)_4^{4-}$ molten complex and $S_2O_7^{2-}$) at 450 °C is displayed in Fig. 6f.

Lowering of the temperature to 420 and 380 °C under SO_2 and O_2 results in the following changes observed in the in situ Raman spectra shown in Figs. 6c and d: (a) lowering of the 942 and 1034 cm^{-1} bands (bands b and c) of $VO_2(SO_4)_2^{3-}$; (b) gradual blue shift of the 1034 cm^{-1} band (band b) due to the V^V=O terminal stretch of $VO_2(SO_4)_2^{3-}$ [13] to 1046 cm^{-1} (band β), where the V^V=O terminal stretch of $(VO)_2O(SO_4)_4^{4-}$ is known to occur [12,14]; (c) strengthening of the 770/830 cm^{-1} broad feature [bands δ and ε due to V–O–V and S–O–V of $(VO)_2O(SO_4)_4^{4-}$] and appearance of bands at 994 and 690 (bands γ and ζ) due to terminal S–O stretch and $\nu_4(SO_4^{2-})$ split component of $(VO)_2O(SO_4)_4^{4-}$ [12,14]; and (d) lowering of the 1078 cm^{-1} $\nu_1(S_2O_7^{2-})$ band (band A′). These observations indicate the presence of increasing $(VO)_2O(SO_4)_4^{4-}$ amounts at lower temperatures in accordance with shifts in equilibrium [5]. This may also be due to lowering of the reaction rate, giving rise to increased lifetimes of the catalytically active $(VO)_2O(SO_4)_4^{4-}$ complex [5]. Increasing the temperature to 480 °C under SO_2 and O_2 restores the observed bands of the in situ Raman spectrum (shown in Fig. 6e) in their initial relative intensities, i.e., same as in Fig. 6b. The most prominent bands due to the various species present are listed in Table 3 (column 3) together with their assignments and are marked by vertical lines in Fig. 6, where lowercase greek letters α–θ denote bands due to $(VO)_2O(SO_4)_4^{4-}$ and A′ denotes the $\nu_1(S_2O_7^{2-})$. A, B, and a–c denote bands due to crystalline Cs_2SO_4 and molten $VO_2(SO_4)_2^{3-}$, as stated above.

Analogous changes are observed in the spectra of the A9Cs and C21Cs V_2O_5–Cs_2SO_4/SiO_2 catalysts under SO_2/O_2 atmosphere, recorded in the same temperature range.

Fig. 7 shows the in situ Raman spectra of the A5Cs catalyst in the presence of SO_2 (0.4% SO_2 in a balance of N_2), i.e., under reducing conditions. Spectrum a in Fig. 7 is obtained at 480 °C after treating the calcined catalyst (Fig. 4b) in SO_2/O_2 atmosphere; thereby the bands due to crystalline Cs_2SO_4 disappear and as discussed in the context of Fig. 6, the features due to $(VO)_2O(SO_4)_4^{4-}$ and $VO_2(SO_4)_2^{3-}$ dominate the spectrum. After stopping the flow of O_2 and gradual lowering of the temperature to 380 °C the following changes are seen in spectra b–d in Fig. 7: (i) the intensity of the 770/830 cm^{-1} characteristic feature due to

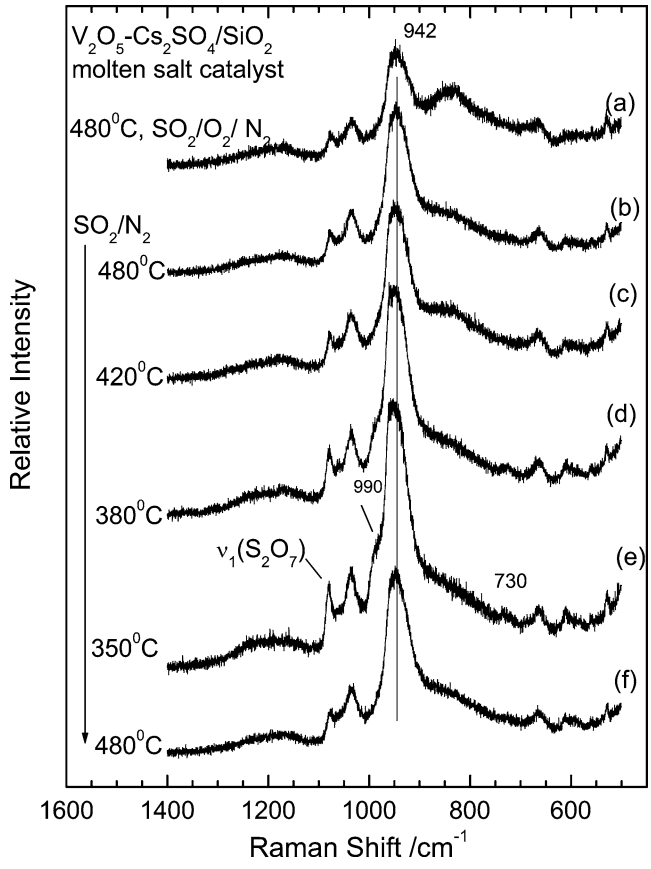

Fig. 7. In situ Raman spectra of V_2O_5–Cs_2SO_4/SiO_2 A5Cs catalyst recorded at temperatures and atmospheres listed by each spectrum. Recording parameters: see Fig. 3.

$(VO)_2O(SO_4)_4^{4-}$ drops significantly when compared to the 942 cm^{-1} band of the $VO_2(SO_4)_2^{3-}$ complex; and (ii) the intensity of the $\nu_1(S_2O_7^{2-})$ 1078 cm^{-1} band is increased and furthermore the second strongest band of molten pyrosulfate at 730 cm^{-1} also emerges in spectrum d (Fig. 7), indicating that in the absence of oxygen in the feed gas, equilibrium (5) is shifted to the left. Furthermore, exposure to SO_2 below 420 °C results in a blue shift of the 942 cm^{-1} band (see, e.g., spectrum d), a fact, which is interpreted to indicate reduction of V^V to V^{IV} molten complexes. The sulfate modes of the formed V^{IV} oxosulfato complexes are the most prominent bands of these species and occur near 965 cm^{-1} [14]. Thus, with increasing extent of vanadium reduction, the combination of the band due to the V^{IV} complexes with the envelope of the 942 cm^{-1} band results in a gradual blue shift of the band observed in this region. The possible $V^V \rightarrow V^{IV}$ reactions taking place in the *molten* phase can be written as [14,18,19]

$$(V^VO)_2O(SO_4)_4^{4-} + SO_2 \rightarrow 2V^{IV}O(SO_4)_2^{2-} + SO_3, \quad (6)$$

$$2V^VO_2(SO_4)_2^{3-} + SO_2 \rightarrow V^{IV}O(SO_4)_2^{2-} + V^{IV}O(SO_4)_3^{4-}. \quad (7)$$

The most prominent bands of the V^{IV} *molten* complexes formed according to reactions (6) and (7) are expected near

965 cm^{-1} [14] (sulfate modes) whereas their V^{IV}=O stretch is expected around 1036 cm^{-1} (where the V^{V}=O stretch occurs) [14].

Further lowering of the temperature to 350 °C results in the appearance of a band at 990 cm^{-1} (spectrum 7e), characteristic of the V^{IV}=O stretch of the vanadyl (VO^{2+}) ion of crystalline vanadium compounds [41]. The formation and precipitation of low-valence vanadium crystalline compounds in V_2O_5-based SO_2 oxidation molten salt catalysts has been shown to take place at temperatures typically below 440 °C [16,17,42]. Previously, the V^{IV} crystalline compounds $Cs_2(VO)_2(SO_4)_3$ and $VOSO_4(SO_2SO_3)_x$ have been isolated from Cs-containing V_2O_5–$Cs_2S_2O_7$ molten salts in reducing (i.e., SO_2) conditions [16,17]. Depending on the catalyst melt composition, the type of alkali promoter and the gas conditions applied, a number of such compounds have been isolated, characterized, and referred to as catalyst deactivation products [5,16,17]. It is evident that the appearance of the 990 cm^{-1} band occurs simultaneously with an increase in the relative intensities of the 1078 and 730 cm^{-1} bands due to the pyrosulfate solvent, $S_2O_7^{2-}$. A possible reaction describing the reduction of the catalytically active V^{V} complex, $(VO)_2O(SO_4)_4^{4-}$, and the formation of the crystalline $Cs_2(V^{IV}O)_2(SO_4)_3$ compound with simultaneous liberation of solvent $S_2O_7^{2-}$ ligands can be written as

$$(V^{V}O)_2O(SO_4)_4^{4-} + SO_2 + 2Cs^{+} \rightarrow Cs_2(V^{IV}O)_2(SO_4)_3(s) + S_2O_7^{2-}. \quad (8)$$

This scheme describes a plausible deactivation route of the SO_2 oxidation catalysts, resulting in depletion of the catalyst melts from their active component, during which vanadium comes out of the molten phase in a nonactive tetravalent state and the remaining liquid contains larger amounts of inactive components (i.e., pyrosulfate).

When the temperature is raised to 480 °C (see spectrum f in Fig. 7) the 990 cm^{-1} disappears, indicating the dissolution of the precipitate, as expected [16,17] and the features of the spectrum 7b (i.e., before cooling in reducing atmosphere) are fully restored.

3.4. Molecular structure of catalysts and relation to catalytic activity

As stated already, nonpromoted V_2O_5/SiO_2 catalysts exhibit very low activity for the SO_2 oxidation reaction. The molecular structure of these catalysts under dehydrated conditions evolves from isolated tetrahedrally distorted O=V–$(O–Si)_3$ monovanadates, to bulk V_2O_5 crystals when vanadia loading exceeds the maximum surface coverage of vanadia on the silica support [34,35]. However, upon impregnation with Cs_2SO_4 and calcination in air, amorphous and crystalline vanadia is “extracted” and dissolved in a sulfate molten salt, which is distributed in the surface of the catalyst carrier. When the impregnation with Cs_2SO_4 is done at a Cs:V = 3 ratio, the predominant molten vanadium oxosulfato complex formed is the mononuclear $VO_2(SO_4)_2^{3-}$ species [13], whereas excess sulfate is identified by means of XRD and Raman spectra (Figs. 1 and 4) in crystalline form. Moreover, during *activation* (i.e., treatment in SO_2/O_2 reacting mixture) the liquid phase takes up SO_3 and a pyrosulfate molten salt is formed, in which the predominant vanadium(V) oxosulfato

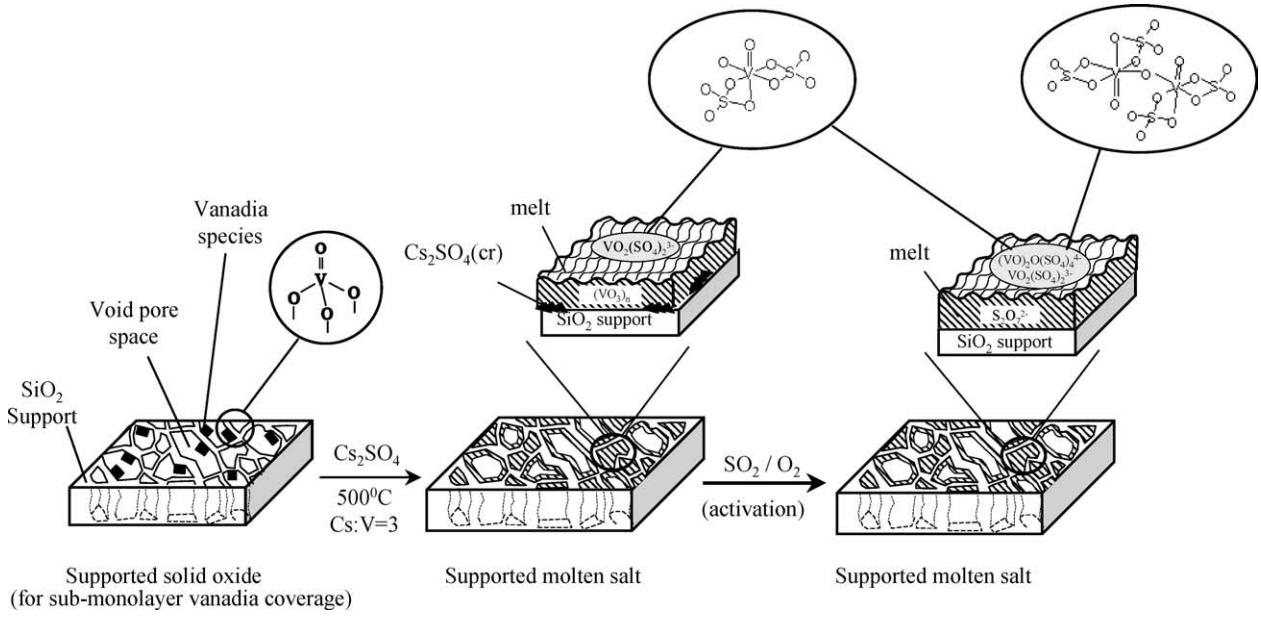

Fig. 8. Schematical representation of proposed structural transformations in V_2O_5/SiO_2 catalysts, following impregnation with Cs_2SO_4, calcination (O_2, 500 °C) and activation in SO_2/O_2 mixture. The scheme shows the molecular structure of the most prominent species.

complex is the dinuclear $(VO)_2O(SO_4)_4^{4-}$ complex [5,12, 14]. A schematical representation of the structural transformations occurring in the nonpromoted V_2O_5/SiO_2 catalyst is proposed in Fig. 8. Vanadia is deposited at the surface of the carrier in the form of tetrahedrally distorted VO_4 species, as shown in Fig. 8a, which depicts the case of a catalyst with submonolayer coverage. The proposed structural models for the vanadium(V) oxosulfato complexes formed in the sulfate and pyrosulfate supported molten salts are shown in schemes b and c. The configurations depicted in Fig. 8 have been proposed earlier, based on high-temperature Raman studies of the V_2O_5–$M_2S_2O_7$–M_2SO_4/O_2–SO_2 unsupported molten salt/gas systems [13,14]. The above-noted complex units do not occur necessarily in isolated form but may participate in oligomeric or polymeric chain-like complex ions [5,13,14]. Thus, vanadium(V) oxosulfato complexes are the prominent species at steady state. Transient experiments [15,43] that were beyond the scope of the present work could shed light on, e.g., whether or not this is due to rapid reoxidation of V^{IV} to V^{V}.

4. Conclusions

Supported solid vanadia/silica catalysts with densities 0.97–2.04 VO_x/nm^2 were found to have very low activity ($\sim 10^{-6}$ s^{-1}) for the reaction of SO_2 oxidation at 400 °C. The molecular structure of these catalysts evolves from isolated distorted tetrahedral O=V–$(O–Si)_3$ monovanadates to bulk V_2O_5 crystals when vanadia exceeds the monolayer surface coverage. Cesium promotion of the catalysts (following impregnation with Cs_2SO_4) and calcination in air or oxygen results in the "extraction" of amorphous and crystalline vanadia from the silica support and their subsequent dissolution in a sulfate molten salt, which remains distributed in the inert support matrix. The molecular structure of the predominant vanadium species in the freshly calcined supported molten salt catalyst is represented by the mononuclear $V^{V}O_2(SO_4)_2^{3-}$ oxosulfato complex. Upon activation of these materials in reacting SO_2/O_2 environment TOF values of the order of 5×10^{-3} s^{-1} for the SO_2 oxidation reaction are obtained. A fairly good correlation between the surface areas of V_2O_5/SiO_2 precursors and the TOF values were found for the V_2O_5–Cs_2SO_4/SiO_2 molten salt catalysts. From a structural point of view, the *active* liquid phase is a pyrosulfate molten salt, in which the predominant species is the catalytically active dinuclear $(V^{V}O)_2O(SO_4)_4^{4-}$ complex. Exposure of the supported molten salt catalysts in reducing atmosphere, i.e., SO_2/N_2, results in accumulation of catalytically inactive V^{IV} complex species. The results are considered useful for designing V_2O_5/SiO_2 SCR catalysts with minimal activities for—the undesirable—SO_2 oxidation and for understanding structure/activity relationships in V_2O_5–Cs_2SO_4/SiO_2-supported molten salt catalysts.

Acknowledgments

NATO's Scientific Affairs Division in the framework of the Science for Peace Programme (SfP 971984) has sponsored this research. Support from the General Secretariat of Research and Technology of the Greek Ministry of Development and from FORTH/ICE-HT is gratefully acknowledged.

References

[1] D.J. Smith (Ed.), Power Eng. Int. ((Apr. 21, 1994));
H. Jensen-Holm, O. Rud-Bendixen, Industrial Experience with the Topsoe VK 48 Sulfuric Acid Catalyst and the WSA-2 Process, presented at Sulfur 1990, Cancun, Mexico.
[2] J. Villadsen, H. Livbjerg, Catal. Rev.-Sci. Eng. 17 (1978) 203.
[3] A. Urbanek, M. Trela, Catal. Rev.-Sci. Eng. 21 (1980) 73.
[4] B.S. Bal'zhinimaev, V.E. Ponomarev, N.P. Belyaeva, A.A. Ivanov, G.K. Boreskov, React. Kinet. Catal. Lett. 30 (1986) 23.
[5] O.B. Lapina, B.S. Bal'zhinimaev, S. Boghosian, K.M. Eriksen, R. Fehrmann, Catal. Today 51 (1999) 469.
[6] N.H. Hansen, R. Fehrmann, N.J. Bjerrum, Inorg. Chem. 21 (1982) 744.
[7] R. Fehrmann, M. Gaune-Escard, N.J. Bjerrum, Inorg. Chem. 25 (1986) 1132.
[8] G. Hatem, R. Fehrmann, M. Gaune-Escard, N.J. Bjerrum, J. Phys. Chem. 91 (1987) 195.
[9] G. Folkmann, G. Hatem, R. Fehrmann, M. Gaune-Escard, N.J. Bjerrum, Inorg. Chem. 32 (1993) 1559.
[10] O.B. Lapina, V.M. Mastikhin, A.A. Shubin, K.M. Eriksen, R. Fehrmann, J. Mol. Catal. A: Chem. 99 (1995) 123.
[11] I. Petrushina, N.J. Bjerrum, F. Cappeln, J. Electrochem. Soc. 145 (1998) 3721.
[12] S. Boghosian, F. Borup, A. Chrissanthopoulos, Catal. Lett. 48 (1997) 145.
[13] S. Boghosian, J. Chem. Soc., Faraday Trans. 94 (1998) 3463.
[14] S. Boghosian, A. Chrissanthopoulos, R. Fehrmann, J. Phys. Chem. B 106 (2002) 49.
[15] B.S. Bal'zhinimaev, A.A. Ivanov, O.B. Lapina, V.M. Mastikhin, K.I. Zamaraev, Faraday Discuss. Chem. Soc. 87 (1989) 133.
[16] S. Boghosian, R. Fehrmann, N.J. Bjerrum, G.N. Papatheodorou, J. Catal. 119 (1989) 121.
[17] K.M. Eriksen, D.A. Karydis, S. Boghosian, R. Fehrmann, J. Catal. 155 (1995) 32.
[18] D.A. Karydis, K.M. Eriksen, R. Fehrmann, S. Boghosian, J. Chem. Soc. Dalton Trans. (1994) 2151.
[19] S.B. Rasmussen, K.M. Eriksen, R. Fehrmann, J. Phys. Chem. B 103 (1999) 11282.
[20] I. Giakoumelou, R.M. Caraba, V. Parvulescu, S. Boghosian, Catal. Lett. 78 (2002) 209.
[21] A. Christodoulakis, S. Boghosian, J. Catal. 215 (2003) 139.
[22] V.I. Parvulescu, P. Grange, B. Delmon, Catal. Today 46 (1998) 233.
[23] H. Bosch, F.J.J.G. Janssen, Catal. Today 2 (1998) 369.
[24] J.P. Dunn, P.R. Koppula, H.G. Stenger, I.E. Wachs, Appl. Catal. B 19 (1998) 103.
[25] H.F.A. Topsoe, A. Nielsen, Trans. Dan. Acad. Tech. Sci. 1 (1947) 18.
[26] F. Doering, D. Berkel, J. Catal. 103 (1987) 126.
[27] R.M. Caraba, S.G. Masters, K.M. Eriksen, V.I. Parvulescu, R. Fehrmann, Appl. Catal. B 34 (2001) 191.
[28] Z. Wang, Q. Liu, J. Yu, T. Wu, G. Wang, Appl. Catal. A 239 (2003) 87.
[29] G.K. Boreskov, A.A. Ivanov, B.S. Balzhinimaev, L.M. Karatovskaya, React. Kinet. Catal. Lett. 14 (1968) 25.
[30] K. Nowinska, Z. Phys. Chem. Neue Folge 126 (1981) 117.

[31] G.K. Boreskov, V.A. Dzis'ko, D.V. Tarasova, G.P. Balaganskaya, Kinet. Katal. 11 (1970) 181.
[32] G.M. Polyakova, G.K. Boreskov, A.A. Ivanov, L.P. Davydova, G.A. Marochkina, Kinet. Katal. 12 (1971) 586.
[33] B.S. Balzhinimaev, V.E. Ponomarev, G.K. Boreskov, A.A. Ivanov, React. Kinet. Catal. Lett. 25 (1984) 219.
[34] I.E. Wachs, B.M. Weckhuysen, Appl. Catal. A 157 (1997) 67.
[35] S. Xie, E. Iglesia, A.T. Bell, Langmuir 16 (2000) 7162.
[36] X. Gao, S.R. Bare, B.M. Weckhuysen, I.E. Wachs, J. Phys. Chem. B 102 (1998) 10842.
[37] P. MacMillan, Am. Miner. 69 (1986) 622.
[38] A. Khodakov, B. Olthof, A.T. Bell, E. Inglesia, J. Catal. 181 (1999) 205.
[39] R.I. Dearnaley, D.H. Kerridge, Thermochim. Acta 63 (1983) 219.
[40] K. Nakamoto, Infrared and Raman Spectra of Inorganic and Coordination Compounds, Wiley, New York, 1986.
[41] J. Selbin, Coord. Chem. Rev. 1 (1966) 293;
Chem. Rev. 65 (1965) 153.
[42] S.G. Masters, A. Chrissanthopoulos, K.M. Eriksen, S. Boghosian, R. Fehrmann, J. Catal. 166 (1997) 16.
[43] A.A. Ivanov, B.S. Bal'zhinimaev, React. Kinet. Catal. Lett. 35 (1987) 413.